Materials Science & Engineering A 692 (2017) 146–155

Contents lists available at ScienceDirect

Materials Science & Engineering A

journal homepage: www.elsevier.com/locate/msea

Influence of thin-film metallic glass coating on fatigue behavior of bulk metallic glass: Experiments and finite element modeling

Chia-Chi Yu[a], Jinn P. Chu[a,*], Haoling Jia[b], Yu-Lin Shen[c], Yanfei Gao[b], Peter K. Liaw[b], Yoshihiko Yokoyama[d]

[a] Department of Materials Science and Engineering, National Taiwan University of Science and Technology, Taipei 10607, Taiwan
[b] Department of Materials Science and Engineering, The University of Tennessee, Knoxville, TN 37996, USA
[c] Department of Mechanical Engineering, University of New Mexico, Albuquerque, NM 87131, USA
[d] Institute for Materials Research, Tohoku University, Sendai 980-8577, Japan

ARTICLE INFO

Keywords:
Metallic glass
Four-point-bend fatigue
Shear band
Finite-element modeling

ABSTRACT

A coating of the Zr-based thin-film metallic glass (TFMG) was deposited on the $Zr_{50}Cu_{30}Al_{10}Ni_{10}$ bulk metallic glass (BMG) to investigate shear-band evolution under four-point-bend fatigue testing. The fatigue endurance-limit of the TFMG-coated samples is ~ 33% higher than that of the BMG. The results of finite-element modeling (FEM) revealed a delay in the shear-band nucleation and propagation in TFMG-coated samples under applied cyclic-loading. The FEM study of spherical indentation showed that the redistribution of stress by the TFMG coating prevents localized shear-banding in the BMG substrate. The enhanced fatigue characteristics of the BMG substrates can be attributed to the TFMG coatings retarding shear-band initiation at defects on the surface of the BMG.

1. Introduction

Bulk metallic glasses (BMGs) have attracted considerable attention as structural materials, due to their high strength, superior elasticity, and high corrosion resistance [1]. However, the applicability of these materials is restricted by poor room-temperature plastic deformability and fatigue properties, which can lead to catastrophic failure under mechanical loading. Brittle fractures in BMGs are associated with the formation of highly-localized shear regions, referred to as shear bands. Crystalline materials are easily susceptible to crack propagation, which greatly undermines their resistance to fatigue [2–5]. Researchers have proposed two mechanisms to explain fatigue-crack initiation in BMGs [6,7]. The first involves the initiation of cracks when the stress is concentrated at casting defects, such as pre-existing pores and inclusions. The second involves the initiation of shear bands from the free surface of the BMGs under cyclic loading. Shear bands accommodate the release of elastic energy and heat, causing the shear regions to weaken into shear steps to produce microcracks under further cyclic loading [8]. Several methods have been proposed to improve the fatigue resistance of BMGs [9–11]. The fatigue mechanisms of BMGs differ considerably from those of crystalline materials, due to differences in their atomic and microscopic structures [7]. The method used to enhance the fatigue-endurance of crystalline materials (shot peening) is inapplicable to glassy alloys. Raghavan et al. [9] determined that during fatigue cycles, stress would concentrate in softened regions or shear bands induced by shot peening, thereby accelerating crack initiation and reducing fatigue resistance. Another approach to improving the fatigue endurance of BMGs involves the introduction of a second phase into the matrix in order to constrain the propagation of shear bands and cracking [10–12]. However, some BMG composites exhibit fatigue lifetime lower than that of monolithic BMGs in the low-cycle-fatigue region, due to the fact that crack propagation occurs more rapidly in the second phase than in the BMG matrix [10,12]. Furthermore, various microstructural characteristics of BMG composites, such as phase size and spacing, are difficult to control. In the current study, we conducted four-point-bend fatigue tests to determine whether a thin coating of metallic glass (~260 nm) could delay shear-band propagation and thereby improve the fatigue characteristics of BMGs.

We determined that the deformation behavior transits from the localized shear banding to homogeneous plastic flow when the sample size is reduced from the millimeter- to nanometer-scales [13–16]. According to Weibull statistics, the strength of small-scale MGs should be higher due to a smaller flaw-size distribution, requiring a higher stress (i.e., more energy) to initiate the formation of shear bands [17,18]. Thin-film metallic glasses (TFMGs) on the sub-micrometer

* Corresponding author.
E-mail address: jpchu@mail.ntust.edu.tw (J.P. Chu).

http://dx.doi.org/10.1016/j.msea.2017.03.071
Received 7 February 2017; Received in revised form 17 March 2017; Accepted 18 March 2017
Available online 21 March 2017

scale provide strength and ductility superior to those of its bulk form [19]. TFMGs have been used to improve the fatigue properties of crystalline materials, including 316 L stainless steels [20], nickel-alloy [21], titanium-alloy [22], and aluminium-alloy [23]. The improved fatigue characteristics can be attributed to the high ductility and strength of the TFMG coatings, which retards fatigue-cracking-initiation in TFMG/substrate materials under cyclic loading. Few studies have reported on efforts to improve the fatigue properties of BMGs through the application of coatings. This is one of the first studies to extend the use of TFMG coatings as a protective layer on crystalline materials in order to improve the fatigue characteristics of BMGs. In this study, we investigated the effects of such coatings on shear-band initiation in BMG substrates during fatigue tests. We did not take into account the evolution of fatigue-crack propagation. We conducted a systematic investigation of shear-band evolution in film/substrate systems using experiments and numerical modeling. We conducted finite-element modeling (FEM) of film/substrate systems under the effects of fatigue and indentation to elucidate the means by which the coatings affect shear-band formation and evolution in BMG substrates.

2. Experimental methods

$Zr_{50}Cu_{30}Al_{10}Ni_{10}$ BMGs (in atomic percent, at%) were machined into rectangular slabs with sample dimensions of 3 mm×3 mm ×25 mm from as-cast ingots fabricated by arc melting under an argon atmosphere. Prior to thin-film deposition, the surfaces of the BMG samples were mechanically polished to a mirror finish. The 260 nm-thick MG films were deposited on the BMG substrates with a $Zr_{55}Cu_{29}Al_{11}Ni_5$ alloy target using radio frequency magnetron sputtering deposition at a base pressure of $< 1\times10^{-6}$ Torr. Argon was introduced as a sputtering gas at a working pressure of 3 mTorr with an applied substrate bias of −50 V.

Four-point bending fatigue tests were conducted on bare and TFMG-coated samples. The experiments were carried out using a Materials Test System (MTS370). The spans of between upper pins and bottom lower pins were 10 mm and 20 mm, respectively. The fatigue tests were performed under in load-control mode on a hydraulic load frame, using sinusoidal waveforms at frequencies of 10 Hz with R =0.1, where R is the ratio of the minimum stress to the maximum stress. Testing was conducted until the sample failed or until a predefined run out of 1×10^7 cycles was attained. The calculations of the nominal maximum alternating stress was obtained, using the following equation: $\sigma=3\times P\times(l\text{-}d)/2\,wt^2$, where P is the applied load, l is the support span, and d is the upper span, and w and t are the width and thickness of the specimens, respectively. The crystallographic structures of the samples were characterized using an X-ray diffractometer (XRD, D8 Discover) with Cu Kα radiation at 40 kV and 200 mA. A low glancing angle was used for analysis of the thin films. The element compositions of the samples was determined employing the energy-dispersive spectrometry (EDS), The fracture surfaces of the specimens were examined using a scanning electron microscope (SEM) with a dual-beam focused ion-beam system (FIB, FEI Quanta 3D FEG). The transmission electron microscope (TEM) foil specimens were prepared with a 30- kV Ga^+ focused ion beam for the initial sectioning, and 5 kV for the final ion polishing. A TEM operated at 200 kV was used to examine the microstructure and to obtain the selected-area electron diffraction (SAED) patterns of the samples.

3. Numerical approaches

The experiments on the TFMG-substrate materials were designed to elucidate the structure and mechanical properties of the thin films as well as substrates. However, the extreme thinness of the films hampered the formulation of stress and strain plots. Furthermore, illustrating the shear-band initiation and propagation in metallic glasses is difficult using experimental methods. Thus, we employed FEM to derive this information.

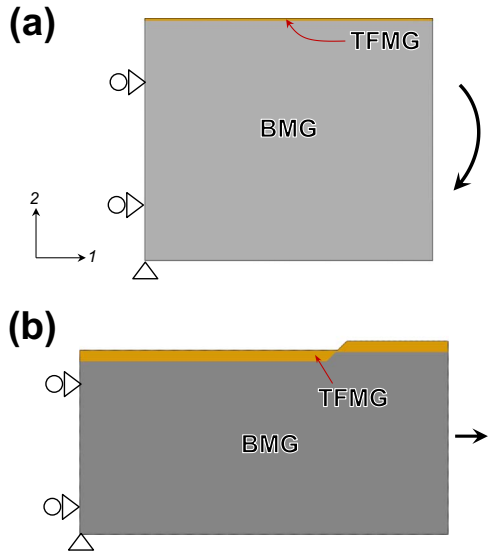

Fig. 1. Numerical models representing (a) the through-thickness segment of the TFMG-coated material under cyclic bending; and (b) the local top segment with the existing shear step under cyclic tension loading.

3.1. Fatigue Model

FEM of uncoated and TFMG-coated BMG substrates is performed, with an aim to rationalize the fatigue behavior observed experimentally. Fig. 1**(a)** illustrates the computational model and boundary conditions employed for the cyclic bending test. The thickness of the TFMG coating is identical to the experimental value, and the substrate thickness is taken as 20 μm. Another case involving only a bare BMG without any coating is also considered. Bending deformation is introduced by imposing displacements along the 1-direction, linearly graded through the thickness, to the right-hand boundary. The maximum bending tensile strain on the top side is set at 0.025. Cyclic deformation between zero strain and this peak value is then simulated. Along the left-hand boundary, displacement in the 1-direction is forbidden during deformation, but movement in the 2-direction is allowed except that the lower-left corner node remains fixed.

In a separate analysis, attention is directed to the effect of an existing shear offset (as observed in the experiment described below) on subsequent deformation. The model features a local region on the top (tensile) side of the fatigue specimen, as shown in Fig. 1**(b)**. The size of the shear step is taken to be 5/6 of the film thickness. Since the analysis is intended for the quantification of the local deformation field around the surface step, the uniform pulling displacement along the 1-direction on the right-hand boundary is imposed. Cyclic loading between the tensile strains of 0 and 0.025 is simulated. As in the bending fatigue model, a pure BMG counterpart of Fig. 1**(b)** is also included in the investigation.

The materials are treated as isotropic elastic-plastic solids. The Young's modulus and Poisson's ratio of BMGs are 108 GPa and 0.37, respectively. Plastic yielding follows the von Mises criterion and incremental flow theory. The choice of appropriate constitutive laws for amorphous alloys has been a topic of active research [1]. Within the continuum framework, plasticity in crystalline metals is generally controlled only by the deviatoric part of the stress tensor. For disordered materials, such as metallic glasses, hydrostatic pressure is expected to influence the yield behavior. Many experimental investigations have concluded that the pressure dependence of plastic deformation is relatively weak (see Ref [1]. for discussion). Some studies specifically showed that the von Mises criterion is adequate for describing the yield response [24,25]. Therefore, for simplicity purposes, the von Mises criterion with perfect plasticity upon yielding at a uniaxial stress of 2.2 GPa is chosen for this part of the modeling study.

A plasticity model alone cannot capture the actual shear banding phenomenon. Thus, for the bending fatigue simulation, we incorporate randomly-generated "weak" points in the BMG substrate to trigger discrete deformation along maximum shear directions. The weak points have the same elastic-plastic properties as the regular BMG material, except for a built-in softening response upon yielding. This approach has been used successfully to numerically study shear-banding phenomena in metallic glasses [26,27]. The Young's modulus, Poisson's ratio, and yield strength of the TFMG coating are taken to be 124 GPa, 0.37, and 2.93 GPa, respectively. Due to its relatively-ductile nature (as discussed extensively below), no weak points are included in the TFMG model. The models depicted in Fig. 1**(a) and (b)** contain a total of 195,000 and 507,500 four-noded elements. The finite element program, Abaqus (version 6.13, Dassault Systèmes Simulia Corp., Providence, RI, USA), is employed for the modeling efforts.

3.2. Indentation Model

As reported in our previous work [7,28–30], the stress fields can be calculated using the continuum plasticity model in FEM, while the continuum plasticity model cannot consider strain localization in MGs. Here, the strain localization will be studied with finite element simulations based on the free volume model, proposed by Spaepen [31], which can be employed to illustrate the explicit history of shear-band nucleation and propagation under indentation.

In the free-volume model, the free volume driven by stress can be increased, which will reduce the viscosity of BMGs, and, therefore, lead to the strain-softening behavior. In the pure shear case, the plastic-strain rate ($\dot{\gamma}^P$) is calculated by [31].

$$\frac{\partial \gamma^P}{\partial t} = 2f \exp\left(-\frac{\alpha \nu^*}{\nu_f}\right)\exp\left(-\frac{\Delta G^m}{k_B T}\right)\sinh\left(\frac{\tau \Omega}{2k_B T}\right) \quad (1)$$

where τ is the shear stress, ν^* is the hard-sphere volume of an atom, ν_f is the average free volume per atom, ΔG^m is the activation energy, f is the frequency of atomic vibration, k_B is the Boltzmann constant, α is a geometric factor of order 1, Ω is the atomic volume, and T is the absolute temperature. Moreover, in Spaepen's model [31], the evolution of free volumes is determined by two competing processes under deformation: a) free-volume creation driven by stress and b) free-volume annihilation dominated by atomic diffusion. Finally, the net change of free volumes can be represented by [31].

$$\frac{\partial \nu_f}{\partial t} = \nu^* f \exp\left(-\frac{\alpha \nu^*}{\nu_f}\right)\exp\left(-\frac{\Delta G^m}{k_B T}\right)\left\{\frac{2\alpha k_B T}{\nu_f E_{\text{eff}}}\left[\cosh\left(\frac{\tau \Omega}{2k_B T}\right) - 1\right] - \frac{1}{n_D}\right\} \quad (2)$$

here, n_D (n_D =3 in the present work) is the number of atomic jumps needed to annihilate a free volume equal to ν^* and the effective elastic modulus is $E_{\text{eff}}=E/3(1-\upsilon)$.

As illustrated in Eqs. (1) and (2), the plastic-strain and free-volume changes of MGs are assumed to be proportional to the shear stresses. This constitutive model allows us to investigate the interaction between shear bands and background-stress fields, which, therefore, can provide the information on the initiation and propagation of shear bands under deformation. To this end, we will adopt the free volume-based constitutive model to capture the shear-banding events, after being implemented into ABAQUS using the user-defined material (UMAT) subroutine in Ref [32].

Three-dimensional (3D) axisymmetric ABAQUS models, consisting of 8-node linear-brick elements with an element type of C3D8, are constructed for indentation loading, with a BMG substrate and a layer of TFMG. As investigated in our previous work [7,19,26], the mechanical behavior of the film/substrate material system is significantly dependent on the adhesion between the film and substrate, including fatigue and plasticity of TFMG-substrate materials. Generally, the better film-substrate adhesion will lead to greater mechanical performance in the TFMG material systems. Therefore, the perfect film-substrate adhesion models, as well as bare BMG substrate models, are employed in the present finite-element models using a rigid Rockwell indenter. More detailed model information can be referred to Ref [7,29].. For the substrate materials, the constitutive parameters are listed as below: $E\Omega/2k_BT$=240, υ=0.33, υ^*/Ω=1,$\nu_f/\alpha\nu^*$ =0.05, n_D =3, and α=0.15. The normalized loading rate can be calculated as:

$$\dot{\gamma} = \frac{\dot{h}}{Rf}\exp\left(\frac{\Delta G^m}{k_B T}\right) = 2.3 \times 10^{-6}\, s^{-1} \quad (3)$$

In the current TFMG-substrate models, same material parameters are assigned to the TFMGs and BMG substrates, except the yield stress. The yield stress values of TFMGs and BMG substrates are given as 1500 MPa and 1000 MPa, respectively, since the TFMG usually has a larger yield stress than the bulk metallic glasses [26].

4. Results and discussion

4.1. Fatigue characteristics

The EDS analysis identified the composition of the sputtered-TFMG as $Zr_{60}Cu_{24}Al_{11}Ni_5$ (in atomic percent). Fig. 2(a) presents X-ray diffraction patterns of the BMG and TFMG, both of which present a broad diffraction hump with 2θ only in a range of 30–45°, corresponding to an amorphous structure. No Bragg peaks associated with crystalline phases were detected.

The S-N data (Please define S-N curves in Section 2) for the bare and TFMG-coated BMG samples are plotted in Fig. 2(b). The maximum

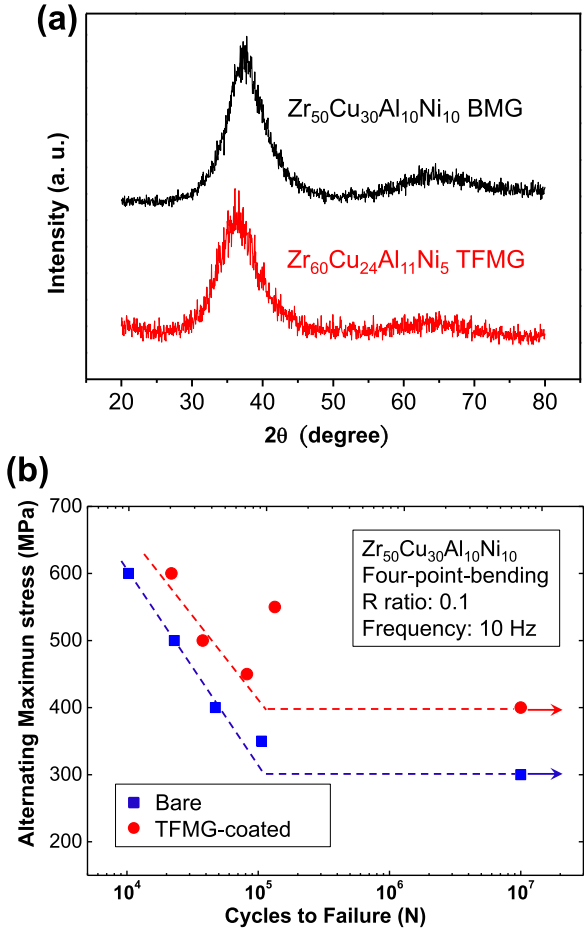

Fig. 2. (a) XRD patterns of the Zr-based TFMG and as-cast $Zr_{50}Cu_{30}Al_{10}Ni_{10}$ BMG; (b) S-N curves of bare and TFMG-coated samples (measured using sinusoidal waveforms at frequencies of 10 Hz with R =0.1).

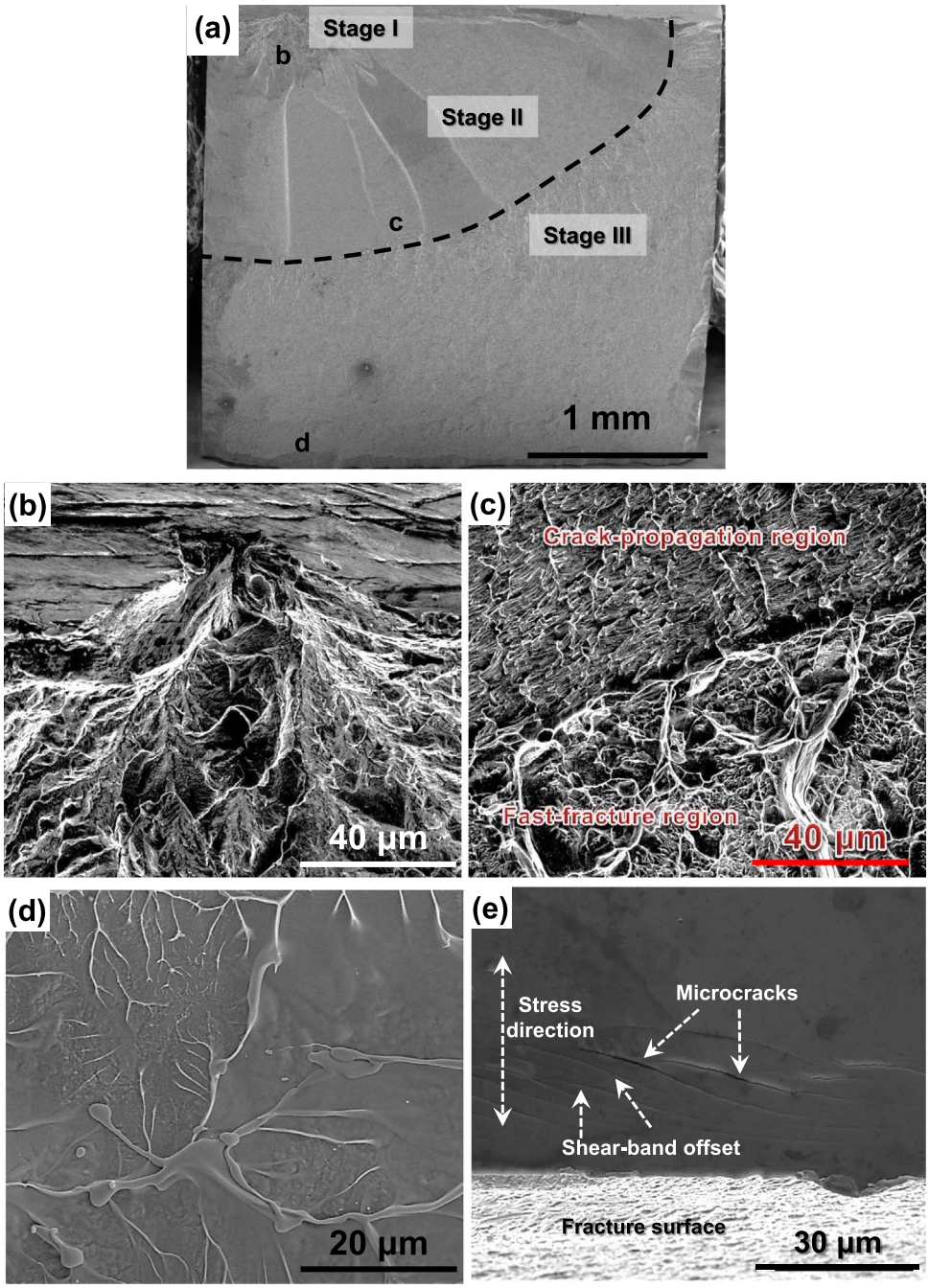

Fig. 3. (a) Fractographic characteristics of TFMG-coated samples tested at σ_{max} of 500 MPa; (b) crack-initiation region; (c) transition region between the crack-propagation region and fast-fracture region; and (d) transition region between the fast-fracture region and melting region; (e) tilted view of the SEM image showing the tensile side of the fractured TFMG-coated sample, revealing micro-cracks and shear-band offsets near the edge of the fracture.

stress range corresponding to 10^7 cycles is defined as the fatigue-endurance limit. As shown in Fig. 2(b), the fatigue-endurance limit of the as-cast BMG samples in this study was 300 MPa. The endurance limit was extended by ~33%, from 300 MPa (the bare BMG) to 400 MPa (the TFMG-coated BMG). The increase in the fatigue-life of the TFMG-coated samples was more pronounced in the region of the low stress fatigue than in regions of the high stress fatigue. This trend is consistent with the characteristics of many TFMG-coated crystalline substrate systems [7,21–23].

4.2. Fractography

The SEM analysis revealed similarities in the fractographic characteristics of the TFMG-coated samples and bare samples, wherein cracks initiated at the tensile surface and then propagated toward the compressive side of the samples. Fig. 3(a) presents the overall fatigue-fractured morphology of the TFMG-coated samples tested under the maximum stress of 500 MPa. BMGs typically present a fracture surface with four distinct regions [6,33]: the fatigue-crack initiation, crack-propagation, fast-fracture, and melting regions. In Fig. 3(b), fatigue cracks initially developed on the tensile surface of the BMG, resulting in striation-type fracturing. As shown in Fig. 3(c), crack initiation is followed by crack propagation in which fatigue-crack growth (with striations) changes to fast fracture (with vein-like patterns). Fig. 3(d) presents the droplets and vein patterns associated with the melting region near the compressive side of BMG specimens. This trend is generally not encountered on the fatigue-fracture surface of crystalline materials. Localized heating can be regarded as the release of the stored

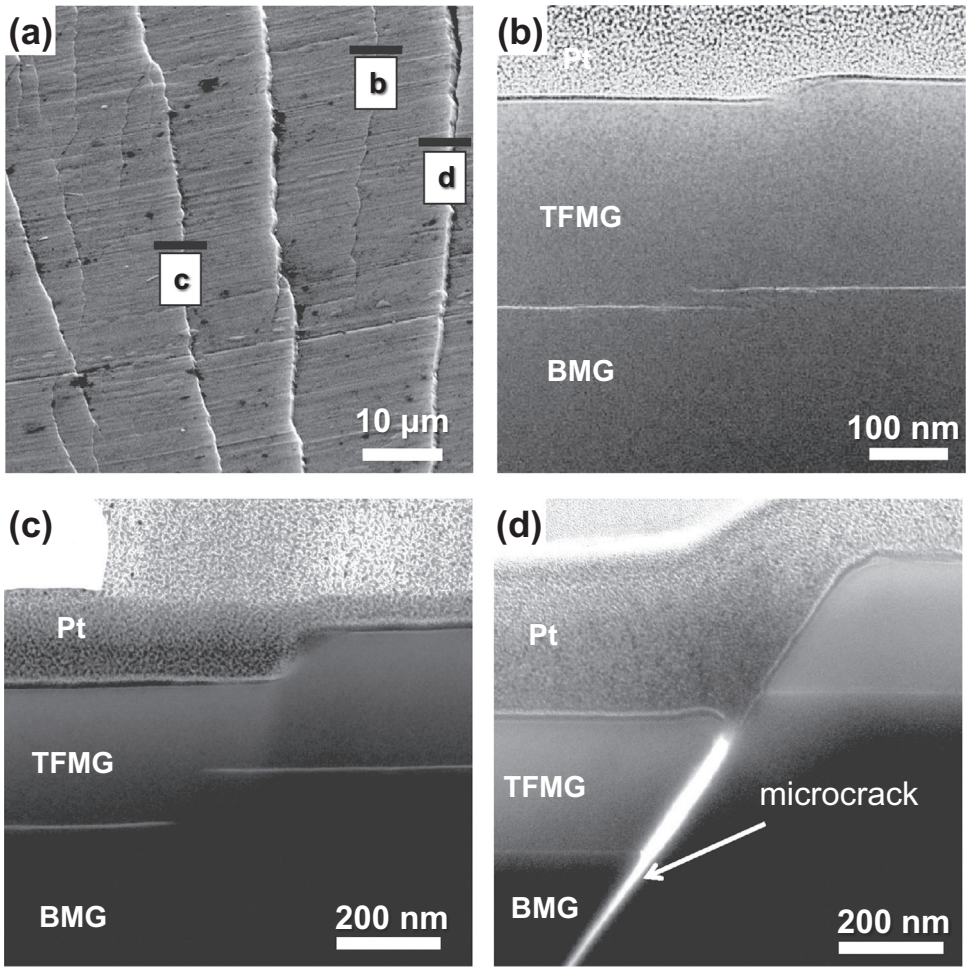

Fig. 4. (a) Tilted view of the SEM image showing the fractured TFMG-coated sample near the edge of the fracture, tested at σ_{max} of 500 MPa. Dark lines indicate the locations used for the preparation of TEM foil samples; (b) to (d) corresponding cross-sectional TEM images with offsets of various heights.

elastic strain energy at the moment of fracture [8]. A fatigue-fractograph of bare BMG sample can be found in Supplementary Fig. S1, which also clearly reveals the stages of fatigue-crack growth. Fig. 3(e) shows a tilted view of the tensile side of the TFMG-coated sample, revealing the micro-cracks and shear-band offset near the edge of the fracture. Microcracks generally initiate from shear-band offsets. Despite the formation of multiple shear-offsets and micro-cracks, the TFMG coating remained strongly adhered to the substrate, with no visible signs of peeling off. Good adhesion between the substrate and coating is a crucial factor influencing the shear-band distribution in TFMG material systems under the effects of deformation [7].

The cross-sectional TEM image of as-deposited TFMG/BMG sample as well as selected-area diffraction patterns for both TFMG coating and BMG substrate can be seen in Supplementary Fig. S2. Fig. 4(a) presents a tilted view of the SEM image of the fractured TFMG-coated sample near the edge of the fracture when tested at σmax =500 MPa. The dark lines indicate locations where the cross-sectional TEM foil samples are prepared. Corresponding TEM images are presented in Fig. 4(b) to (d), respectively. Fig. 4(b) to (d) reveal the evolution of fatigue fractures in the BMG, beginning with the initiation of shear bands on the surface of the sample. The concentration of stress caused the evolution of the shear bands into shear-band offsets, which grew rapidly under further cyclic loading. The shear-band offsets eventually developed into fatigue cracks. The sequential process from shear-banding to the formation of microcracks in Fig. 4 verifies the mechanism of fatigue-crack initiation proposed by Wang et al. [6]. The TFMG coating remained strongly adhered to the BMG substrate, with no signs of delamination or fracturing despite the effects of the film being pulled by the shear steps, indicated by the homogeneous plastic deformation. As shown in Fig. 4(c), the TFMG coating was able to withstand the considerable shear strain, showing indications of interdiffusion with BMGs at the TFMG/BMG interface along the shear step, as previously reported [34].

Shear bands and/or cracking usually initiate from casting defects and pores introduced during alloy casting. This trend leads to preliminary failure due to differences in the concentration of stress at these sites [35]. Such defects can have a considerable effect on the mechanical properties of BMG specimens, particularly the fatigue characteristics [36,37]. The fact that fatigue cracking begins at shear bands means that the fatigue life of BMGs could be extended simply by delaying shear-band initiation. In fatigue experiments, the initiation of localized shear bands produced shear-softening regions that served as stress concentrators capable of inducing severely-localized shear banding. The resulting shear-band offsets easily evolve into microcracks, which can cause the catastrophic failure. TFMG coatings can be used to compensate for existing flaws on the surface of BMGs. This feature minimizes the formation of stress concentrators and, thereby, extends the fatigue life of the BMG.

4.3. Numerical Modeling Results

4.3.1. Bending-Fatigue Model

The primary objective of this model was to gain qualitative insight into the means by which the TFMG coating improves the fatigue resistance of the BMG. Fig. 5(a) presents a contour plot of equivalent plastic strains in the uncoated BMG substrate at the peak point of the

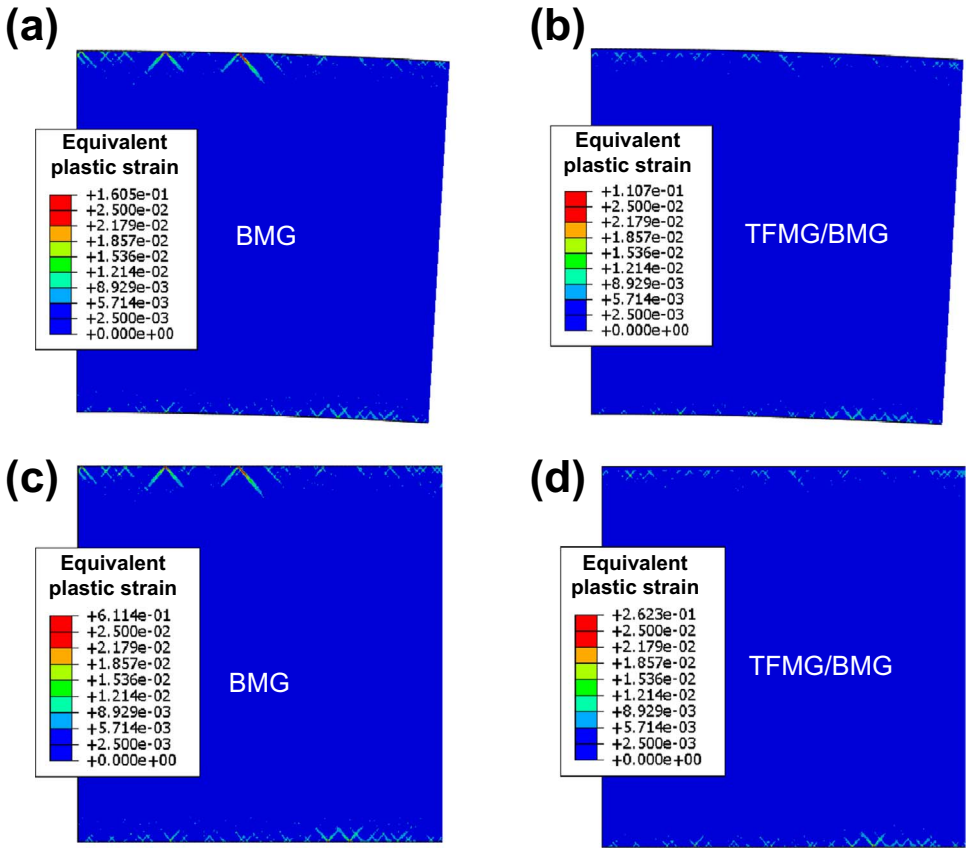

Fig. 5. Contour plots of equivalent plastic strains showing simulations of shear-band configuration: (a) bare BMG and (b) TFMG-coated BMG under the peak load of the first bending cycle, and (c) bare BMG, and (d) TFMG-coated BMG after 5 full bending cycles.

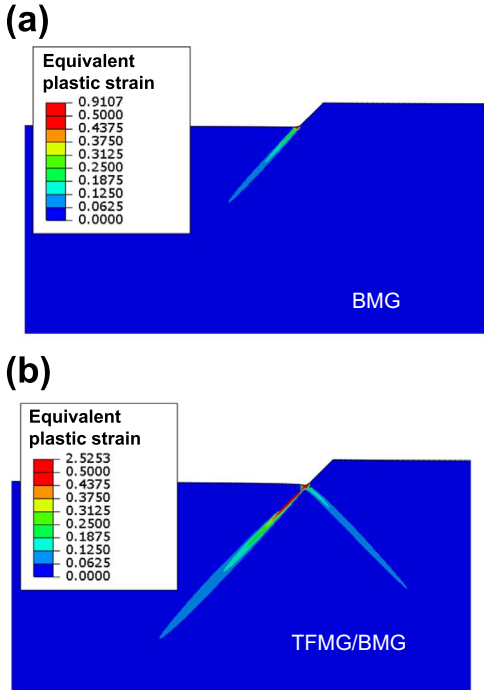

Fig. 6. Contour plots of equivalent plastic strains in (a) bare BMG and (b) TFMG-coated BMG, both with an existing shear step, after 5 full tensile loading cycles. The model in (c) is the same as (b) except for the replacement of the 45° interface between the TFMG and BMG with a graded interface showing a gradual change in material properties.

first bending cycle. Distinct shear bands near the top (tensile) and bottom (compressive) surfaces are apparent. The bands are oriented at 45° to the surface, along the direction of the maximum shear strain. Fig. 5(b) presents the corresponding plot for the TFMG-coated model. The deformation curvature and high shear band density were also observed in the coated specimen. The figure also reveals that the deformation bands are shorter and far less developed in the coated samples than in the bare BMG substrate. It appears that reducing the number of initiation points on the tensile surface of the coated samples limited the localization of deformation; i.e., the coatings partially absorb the deformation energy. As a result, the nucleation of shear bands beneath the interface between the TFMG coating and BMG was more homogeneous, such that discrete patterns were less conspicuous.

Fig. 5(c) and (d), respectively, present contour plots of equivalent plastic strains in the bare BMG and TFMG-coated BMG models after 5 full-bending cycles. These patterns are similar to those shown in Fig. 5(a) and (b). However, the maximum strain values in the cycled models are far higher than those of in the first bending cycle. A comparison between Fig. 5(c) and (d) visually illustrates the large effect that even a thin coating can have on the development of the inhomogeneous deformation patterns. The smaller size and lower strain levels associated with the shear bands in the coated samples suggests that fracturing would be delayed during the fatigue process. This conclusion is in agreement with our experimental observations.

The microscope image in Fig. 4 shows clear evidence of shear offsets on the tensile surface, leading to the formation of microcracks. Thus, we sought to determine the means by which an existing shear offset influences local deformation, with and without the TFMG coating. We used a model depicted in Fig. 1(b) for this purpose. Fig. 6(a) and (b), respectively, exhibit contour plots of equivalent plastic strains in bare BMG and TFMG-coated BMG models after 5 full-loading cycles.

The image shows strong plastic bands emerging from the root of the shear step at an angle of 45°. The coated structure in Fig. 6(b) displays a larger band size with higher strain values, which suggests that failure initiation will occur more readily. Without the possibility of failure in the numerical model, a second band with less pronounced plastic strains was also seen to have developed in the TFMG-coated specimen. The results demonstrated that, once a shear offset has formed, the TFMG coating is no longer able to protect the BMG substrate and may actually promote fracture. Thus, we believe that the improvement in fatigue resistance provided by the coating is due to the more homogeneous deformation (with less plastic localization) underneath the TFMG/BMG interface, which helps delay the formation of dominant shear bands and subsequent formation of shear offsets.

4.3.2. Indentation Model

Fig. 7 presents the 3D axisymmetric indentation model with free-volume contour plots of BMG specimens: (a) bare, (b) with TFMG coating, and (c) with Ti coating. Note that SDV1 in Fig. 7 denotes the first solution-dependent state variable (SDV), which is used to represent the free volume in the UMAT code. Fig. 7(a) shows four pairs of major shear bands that appeared in the bare BMG substrate model under the effects of indentation. Thus, the propagation of major shear bands throughout the entire bare BMG specimen renders the sample highly susceptible to the deformation-induced failure under the effects of indentation. However, the TFMG in Fig. 7(b) reveals minor shear bands appearing in the region proximal to the TFMG-substrate interface, as well as two pairs of major shear bands. From this trend, we can deduce that under the effects of indentation, the load can be shared by minor shear bands, leading to an overall reduction in the stress of the BMG substrates. To investigate the stress sharing in film-substrate (BMG) materials, we formulated an additional 3D indentation axisymmetric model [Fig. 7(c)] to study strain localization in a BMG metallic glass substrate coated with a thin film of Ti, wherein the Ti was treated as a purely elastic body with a Young's modulus of E =122 GPa and a Poisson ratio of υ=0.34. As shown in Fig. 7(c), this model presents a larger number of minor shear bands than that observed in either the bare BMG or TFMG-substrate (BMG) models. This trend means that a layer of Ti could be used to improve the mechanical behavior of bare BMG specimens. However, the benefits are not as pronounced as those afforded by TFMGs.

To verify this hypothesis, we obtained the stress contours of a 3D axisymmetric indentation model on the bare BMG specimens (a) with the TFMG coating (b) and the Ti coating (c). Fig. 8(a) shows the stress evenly concentrated around the major shear bands. In contrast, the TFMG-substrate model [Fig. 8(b)] shows the stress concentrated mainly in the TFMG, which means that the load under indentation is shared by the TFMGs. The stress contour from the Ti-substrate model in Fig. 8(c) shows the stress evenly distributed around the shear-banding region, but with stress values far lower than those of the bare BMG substrate. This feature provides further evidence that Ti thin films slightly improve the mechanical performance of BMG specimens. However, the effect is less than that of TFMGs.

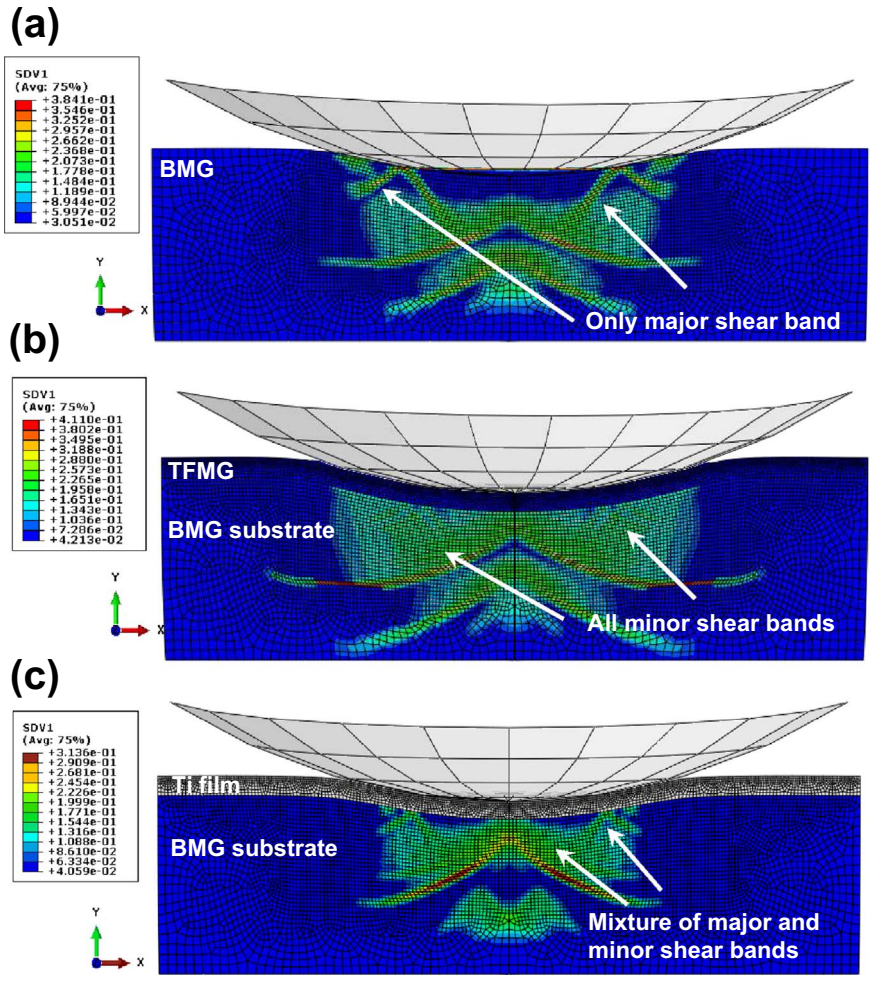

Fig. 7. 3D axisymmetric indentation model using a rigid Rockwell indenter: free-volume contour plots of BMG specimens: (a) bare, (b) with TFMG coating, and (c) with titanium coating.

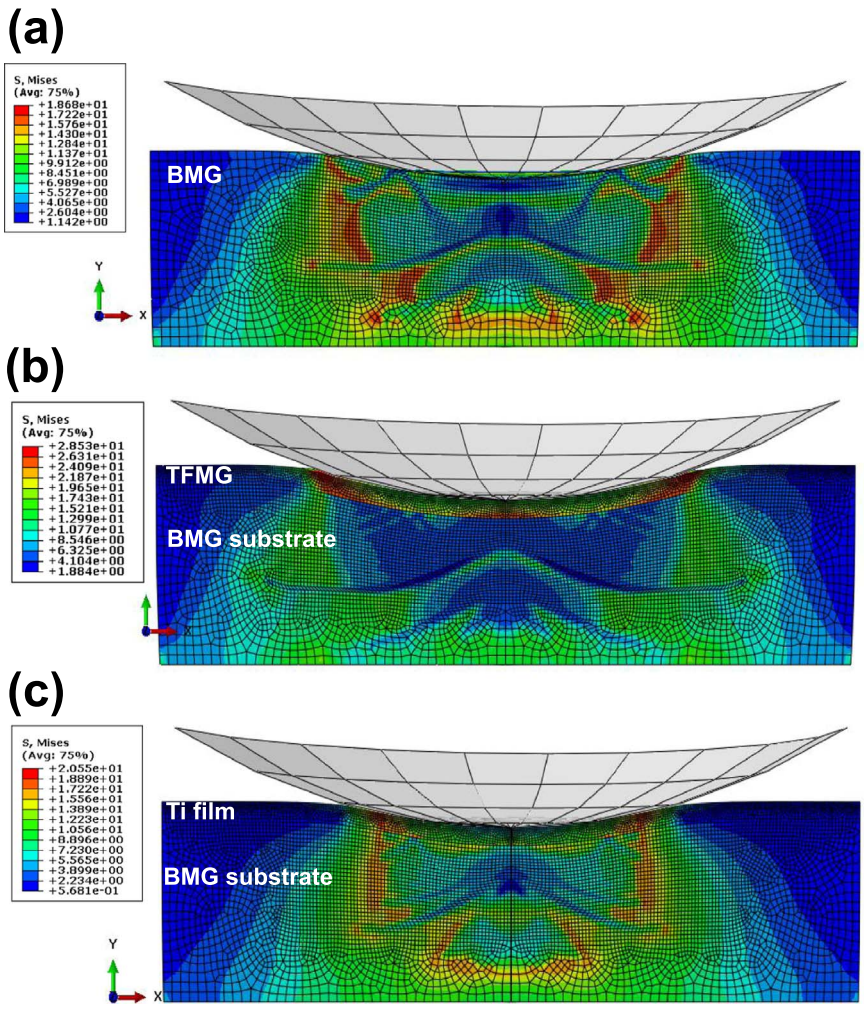

Fig. 8. 3D axisymmetric indentation model using a rigid Rockwell indenter: stress contour plots of BMG specimens: (a) bare, (b) with TFMG coating, and (c) with titanium coating.

4.4. Fatigue-crack-initiation mechanism of the TFMG/BMG system

Several studies have reported improvements in the fatigue properties of crystalline material via the application of TFMG coatings [20,22,23]. Fatigue-crack initiation in a film/substrate system has been attributed to the TFMG coating suppressing the pile-up of dislocations in crystalline materials [21]. The absence of crystalline defects means that fatigue cracking in BMGs is initiated by the growth of shear bands. We observed a similar mechanism in the proposed TFMG/BMG system. Based on the experimental observations and modeling results, we propose that fatigue-crack initiation in the TFMG/BMG system is a three-stage process, as schematically illustrated in Fig. 9. The influence of the TFMG coating on fatigue resistance is apparent only in the first stage, during which it can compensate for defects on the surface of the substrate. Our indentation model indicates that the TFMG coating enables the redistribution of stress (i.e., reduces stress concentration), which helps delay the formation of shear bands and prevents shear localization. Once the shear band transforms into shear steps (stage II), the TFMG coating is no longer able to protect the substrate due to the severe localization of the stress at the film/substrate interface, as shown in Fig. 6(b) and (c). The shear steps continue growing and eventually evolve into microcracks (stage III), whereupon fatigue cracks propagate through the substrate, resulting in the rapid failure of the TFMG/BMG system. Unlike the BMG-composite with crystalline phases, which hinder the shear-band/crack propagation, a strong and ductile TFMG coating can effectively delay the shear-band initiation so as to improve the fatigue properties of BMGs.

5. Conclusion

This study demonstrated conclusively that the fatigue properties of the $Zr_{50}Cu_{30}Al_{10}Ni_{10}$ BMG can be improved through the application of a thin film metallic glass. We systematically investigated the effects of the TFMG coating on the mechanical behavior of a BMG substrate, by conducting fatigue and nanoindentation tests as well as ABAQUS simulations. The conclusions of the presentwork are summarized as follows:

(1) In experiments, the endurance limit (400 MPa) of TFMG-coated samples far exceeded that of bare samples (300 MPa). These findings confirm that delaying shear-band initiation through the application of a TFMG coating enhanced fatigue resistance.
(2) The results of indentation modeling revealed that much of the indentation-related stress was shared by the TFMG coating, which resulted in the formation of only minor shear bands in the BMG substrate. In contrast, the concentration of the stress in the BMG substrate led to the formation of large, localized shear bands in the bare BMG and Ti-coated specimens.
(3) Based on the modeling and experimental results, we propose the following mechanism to explain fatigue-crack initiation in the TFMG/BMG system. The TFMG coating prevents the stress localization at defects on the surface of the BMG surface mainly during the shear-band-initiation stage, thereby delaying the formation of dominant shear bands and subsequent shear offsets.
(4) The ability of the TFMG coating to retard shear-band initiation and

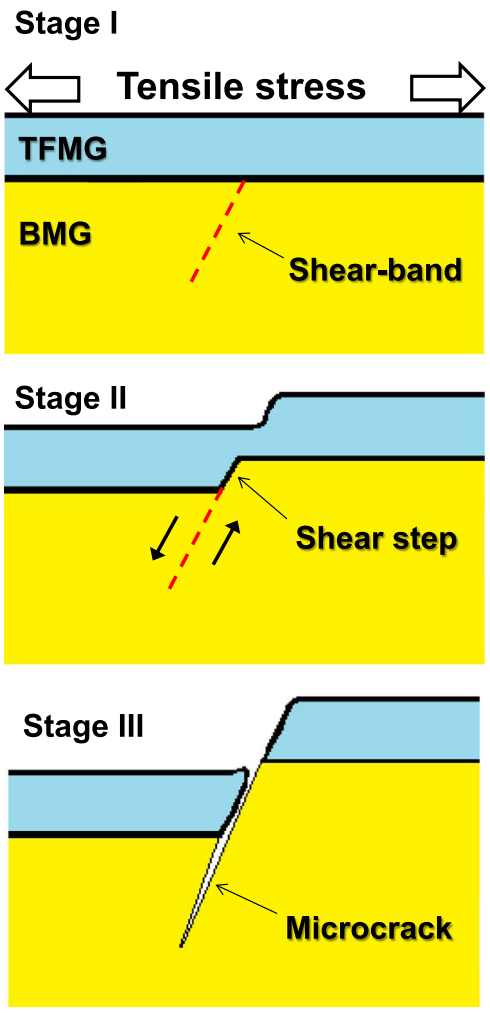

Fig. 9. Schematic illustration showing three-stage fatigue-crack initiation in TFMG/BMG system.

propagation in the BMG substrate during fatigue tests can be attributed primarily to the excellent toughness and plasticity characteristics.

Acknowledgements

The authors gratefully acknowledge the support from the Ministry of Science and Technology of Taiwan under the project number of MOST 104–2218-E-011–018. YFG is supported by the US Department of Energy, Office of Science, Basic Energy Sciences, Materials Sciences and Engineering Division. PKL would like to acknowledge the Department of Energy (DOE), Office of Fossil Energy, National Energy Technology Laboratory (DE-FE-0008855 and DE-FE-0024054, and DE-FE-0011194), with Mr. V. Cedro and Mr. R. Dunst as program managers. PKL thank the support from the project of DE-FE-0011194 with the program manager, Dr. J. Mullen. PKL very much appreciates the support of the U.S. Army Research Office project (W911NF-13-1-0438) with the program manager, Dr. D. M. Stepp. PKL thanks the support from the National Science Foundation (CMMI-1100080 and DMR-1611180) with the program directors, Dr. C. Cooper and D. Farkas.

Appendix A. Supporting information

Supplementary data associated with this article can be found in the online version at doi:10.1016/j.msea.2017.03.071.

References

[1] C.A. Schuh, T.C. Hufnagel, U. Ramamurty, Mechanical behavior of amorphous alloys, Acta Mater. 55 (12) (2007) 4067–4109.
[2] B.C. Menzel, R.H. Dauskardt, Stress-life fatigue behavior of a Zr-based bulk metallic glass, Acta Mater. 54 (4) (2006) 935–943.
[3] G.Y. Wang, P.K. Liaw, M.L. Morrison, Progress in studying the fatigue behavior of Zr-based bulk-metallic glasses and their composites, Intermetallics 17 (8) (2009) 579–590.
[4] Y. Yue, R. Wang, D.Q. Ma, J.F. Tian, X.Y. Zhang, Q. Jing, M.Z. Ma, R.P. Liu, Fatigue behavior of a Zr-based bulk metallic glass under uniaxial tension–tension and three-point bending loading mode, Intermetallics 60 (2015) 86–91.
[5] G.Y. Wang, D.C. Qiao, Y. Yokoyama, M. Freels, A. Inoue, P.K. Liaw, Effects of loading modes on the fatigue behavior of Zr-based bulk-metallic glasses, J. Alloy. Compd. 483 (1–2) (2009) 143–145.
[6] G.Y. Wang, P.K. Liaw, W.H. Peter, B. Yang, Y. Yokoyama, M.L. Benson, B.A. Green, M.J. Kirkham, S.A. White, T.A. Saleh, R.L. McDaniels, R.V. Steward, R.A. Buchanan, C.T. Liu, C.R. Brooks, Fatigue behavior of bulk-metallic glasses, Intermetallics 12 (7–9 SPEC. ISS.) (2004) 885–892.
[7] H. Jia, F. Liu, Z. An, W. Li, G. Wang, J.P. Chu, J.S.C. Jang, Y. Gao, P.K. Liaw, Thin-film metallic glasses for substrate fatigue-property improvements, Thin Solid Films 561 (0) (2014) 2–27.
[8] C.T. Liu, L. Heatherly, D.S. Easton, C.A. Carmichael, J.H. Schneibel, C.H. Chen, J.L. Wright, M.H. Yoo, J.A. Horton, A. Inoue, Test environments and mechanical properties of Zr-base bulk amorphous alloys, Metall. Mater. Trans. A: Phys. Metall. Mater. Sci. 29 (7) (1998) 1811–1820.
[9] R. Raghavan, R. Ayer, H.W. Jin, C.N. Marzinsky, U. Ramamurty, Effect of shot peening on the fatigue life of a Zr-based bulk metallic glass, Scr. Mater. 59 (2) (2008) 167–170.
[10] D.C. Qiao, G.J. Fan, P.K. Liaw, H. Choo, Fatigue behaviors of the Cu47.5Zr47.5Al5 bulk-metallic glass (BMG) and Cu47.5Zr38Hf9.5Al5 BMG composite, Int. J. Fatigue 29 (12) (2007) 2149–2154.
[11] K.M. Flores, W.L. Johnson, R.H. Dauskardt, Fracture and fatigue behavior of a Zr–Ti–Nb ductile phase reinforced bulk metallic glass matrix composite, Scr. Mater. 49 (12) (2003) 1181–1187.
[12] G.Y. Wang, P.K. Liaw, A. Peker, M. Freels, W.H. Peter, R.A. Buchanan, C.R. Brooks, Comparison of fatigue behavior of a bulk metallic glass and its composite, Intermetallics 14 (8–9) (2006) 1091–1097.
[13] H. Guo, P.F. Yan, Y.B. Wang, J. Tan, Z.F. Zhang, M.L. Sui, E. Ma, Tensile ductility and necking of metallic glass, Nat. Mater. 6 (10) (2007) 735–739.
[14] O.V. Kuzmin, Y.T. Pei, C.Q. Chen, J.T.M. De Hosson, Intrinsic and extrinsic size effects in the deformation of metallic glass nanopillars, Acta Mater. 60 (3) (2012) 889–898.
[15] B.E. Schuster, Q. Wei, T.C. Hufnagel, K.T. Ramesh, Size-independent strength and deformation mode in compression of a Pd-based metallic glass, Acta Mater. 56 (18) (2008) 5091–5100.
[16] X. Zhou, H. Zhou, X. Li, C. Chen, Size effects on tensile and compressive strengths in metallic glass nanowires, J. Mech. Phys. Solids 84 (2015) 130–144.
[17] A.L. Greer, Y.Q. Cheng, E. Ma, Shear bands in metallic glasses, Mater. Sci. Eng.: R: Rep. 74 (4) (2013) 71–132.
[18] C.C. Wang, J. Ding, Y.Q. Cheng, J.C. Wan, L. Tian, J. Sun, Z.W. Shan, J. Li, E. Ma, Sample size matters for Al88Fe7Gd5 metallic glass: smaller is stronger, Acta Mater. 60 (13–14) (2012) 5370–5379.
[19] J.P. Chu, J.S.C. Jang, J.C. Huang, H.S. Chou, Y. Yang, J.C. Ye, Y.C. Wang, J.W. Lee, F.X. Liu, P.K. Liaw, Y.C. Chen, C.M. Lee, C.L. Li, C. Rullyani, Thin film metallic glasses: unique properties and potential applications, Thin Solid Films 520 (16) (2012) 5097–5122.
[20] C.L. Chiang, J.P. Chu, F.X. Liu, P.K. Liaw, R.A. Buchanan, A 200 nm thick glass-forming metallic film for fatigue-property enhancements, Appl. Phys. Lett. 88 (13) (2006) 131902.
[21] F.X. Liu, P.K. Liaw, W.H. Jiang, C.L. Chiang, Y.F. Gao, Y.F. Guan, J.P. Chu, P.D. Rack, Fatigue-resistance enhancements by glass-forming metallic films, Mater. Sci. Eng.: A 468–470 (0) (2007) 246–252.
[22] C.M. Lee, J.P. Chu, W.Z. Chang, J.W. Lee, J.S.C. Jang, P.K. Liaw, Fatigue property improvements of Ti–6Al–4V by thin film coatings of metallic glass and TiN: a comparison study, Thin Solid Films 561 (0) (2014) 33–37.
[23] Y.Z. Chang, P.H. Tsai, J.B. Li, H.C. Lin, J.S.C. Jang, C. Li, G.J. Chen, Y.C. Chen, J.P. Chu, P.K. Liaw, Zr-based metallic glass thin film coating for fatigue-properties improvement of 7075-T6 aluminum alloy, Thin Solid Films 544 (0) (2013) 331–334.
[24] H. Kimura, T. Masumoto, Amorph. Met. Alloy. (1983) 87.
[25] H.A. Bruck, T. Christman, A.J. Rosakis, W.L. Johnson, Quasi-static constitutive behavior of Zr41.25Ti13.75Ni10Cu12.5Be22.5 bulk amorphous alloys, Scr. Metall. Et. Mater. 30 (4) (1994) 429–434.
[26] J.P. Chu, J.E. Greene, J.S.C. Jang, J.C. Huang, Y.-L. Shen, P.K. Liaw, Y. Yokoyama, A. Inoue, T.G. Nieh, Bendable bulk metallic glass: effects of a thin, adhesive, strong, and ductile coating, Acta Mater. 60 (6–7) (2012) 3226–3238.
[27] D.N. Rogers, Y.L. Shen, Deformation localization in constrained layers of metallic glasses: a parametric modeling analysis, Thin Solid Films 561 (0) (2014) 108–113.
[28] Z.N. An, W.D. Li, F.X. Liu, P.K. Liaw, Y.F. Gao, Interface constraints on shear band patterns in bonded metallic glass films under microindentation, Metall. Mater. Trans. A 43 (8) (2012) 2729–2741.
[29] H.L. Jia, L.L. Zheng, W.D. Li, N. Li, J.W. Qiao, G.Y. Wang, Y. Ren, P.K. Liaw, Y. Gao, Insights from the lattice-strain evolution on deformation mechanisms in metallic-glass-matrix composites, Metall. Mater. Trans. A 46 (6) (2015)

2431–2442.
[30] L.L. Zheng, Y.F. Gao, S.Y. Lee, R.I. Barabash, J.H. Lee, P.K. Liaw, Intergranular strain evolution near fatigue crack tips in polycrystalline metals, J. Mech. Phys. Solids 59 (11) (2011) 2307–2322.
[31] F. Spaepen, A microscopic mechanism for steady state inhomogeneous flow in metallic glasses, Acta Metall. 25 (4) (1977) 407–415.
[32] Y.F. Gao, An implicit finite element method for simulating inhomogeneous deformation and shear bands of amorphous alloys based on the free-volume model, Model. Simul. Mater. Sci. Eng. 14 (8) (2006) 1329–1345.
[33] M.L. Morrison, R.A. Buchanan, P.K. Liaw, B.A. Green, G.Y. Wang, C.T. Liu, J.A. Horton, Four-point-bending-fatigue behavior of the Zr-based Vitreloy 105 bulk metallic glass, Mater. Sci. Eng.: A 467 (1–2) (2007) 190–197.
[34] C.-C. Yu, C.M. Lee, J.P. Chu, J.E. Greene, P.K. Liaw, Fracture-resistant thin-film metallic glass: ultra-high plasticity at room temperature, APL Mater. 4 (11) (2016) 116101.
[35] Y.Q. Cheng, E. Ma, Intrinsic shear strength of metallic glass, Acta Mater. 59 (4) (2011) 1800–1807.
[36] G.Y. Wang, P.K. Liaw, Y. Yokoyama, A. Inoue, C.T. Liu, Fatigue behavior of Zr-based bulk-metallic glasses, Mater. Sci. Eng.: A 494 (1) (2008) 314–323.
[37] G.Y. Wang, P.K. Liaw, A. Peker, B. Yang, M.L. Benson, W. Yuan, W.H. Peter, L. Huang, M. Freels, R.A. Buchanan, C.T. Liu, C.R. Brooks, Fatigue behavior of Zr–Ti–Ni–Cu–Be bulk-metallic glasses, Intermetallics 13 (3–4) (2005) 429–435.